

Optical properties of SiV and GeV color centers in nanodiamonds under hydrostatic pressures up to 180 GPa

Baptiste Vindolet,^{1,*} Marie-Pierre Adam¹, Loïc Toraille^{1,2,3}, Mayeul Chipaux^{4,†}, Antoine Hilberer¹, Géraud Dupuy,¹ Lukas Razinkovas⁵, Audrius Alkauskas⁵, Gergő Thiering⁶, Adam Gali^{6,7}, Mary De Feudis^{8,‡}, Midrel Wilfried Ngandeu Ngambou⁸, Jocelyn Achard⁸, Alexandre Tallaire,⁸ Martin Schmidt¹, Christoph Becher⁴ and Jean-François Roch^{1,§}

¹Université Paris-Saclay, CNRS, ENS Paris-Saclay, CentraleSupélec, LuMIn, F-91190 Gif-sur-Yvette, France

²CEA DAM DIF, F-91297 Arpajon, France

³Université Paris-Saclay, CEA, Laboratoire Matière en Conditions Extrêmes, 91680 Bruyères-le-Châtel, France

⁴Fachrichtung Physik, Universität des Saarlandes, Campus E2.6, 66123 Saarbrücken, Germany

⁵Center for Physical Sciences and Technology (FTMC), Vilnius LT-10257, Lithuania

⁶Institute for Solid State Physics and Optics, Wigner Research Centre for Physics, P.O. Box 49, H-1525 Budapest, Hungary

⁷Department of Atomic Physics, Institute of Physics, Budapest University of Technology and Economics, Műgyetem rakpart 3, H-1111 Budapest, Hungary

⁸Laboratoire des Sciences des Procédés et des Matériaux, CNRS, Université Sorbonne Paris-Nord, F-93340 Villetaneuse, France



(Received 20 September 2022; accepted 29 November 2022; published 19 December 2022)

We investigate the optical properties of silicon-vacancy (SiV) and germanium-vacancy (GeV) color centers in nanodiamonds under hydrostatic pressure up to 180 GPa. The nanodiamonds were synthesized by Si- or Ge-doped plasma-assisted chemical vapor deposition and, for our experiment, pressurized in a diamond anvil cell. Under hydrostatic pressure we observe blueshifts of the SiV and GeV zero-phonon lines by 17 THz (70 meV) and 78 THz (320 meV), respectively. These measured pressure-induced shifts are in good agreement with *ab initio* calculations that take into account the lattice compression based on the equation of state of diamond and that are extended to the case of the tin-vacancy (SnV) center. This work provides guidance on the use of group-IV-vacancy centers as quantum sensors under extreme pressures that will exploit their specific optical and spin properties induced by their intrinsic inversion-symmetric structure.

DOI: [10.1103/PhysRevB.106.214109](https://doi.org/10.1103/PhysRevB.106.214109)

I. INTRODUCTION

Quantum sensing consists in using quantum systems to perform measurement of given physical quantities [1]. Among the various systems that have been developed, the nitrogen-vacancy (NV) center in diamond has been used to demonstrate and implement a broad variety of sensing protocols, in particular, for the measurement of magnetic and electric fields, and also for the detection of stress, temperature, mechanical vibrations, and fluctuating electromagnetic fields [2]. Due to the stiffness of the hosting diamond crystal, the NV center is also offering a powerful solution for probing matter at the extreme static pressures that are routinely achieved in a diamond anvil cell (DAC) consisting of two anvils that squeeze the sample between their flattened tips [3], as shown in Fig. 1(a). In order

to push the pressure limits, the pressure amplification of the DAC is optimized, essentially by reducing the culet diameter and then putting a constraint on the sample size. For pressures above 100 GPa this leads to sample chambers of less than 50 μm diameter and to the corresponding experimental difficulties in handling and signal detection. Using the optically detected magnetic resonance (ODMR) of the NV electronic spin that can be recorded by collecting the luminescence of the NV centers through the diamond anvil, recent works have shown the applicability of NV-based optical magnetometry to micrometer-sized samples under pressure and external magnetic fields [4–6]. Since the NV centers can be placed in close proximity to the sample, the NV-based detection can be used to map the magnetic field distribution created by the sample magnetization, with a micrometer spatial resolution and with a sensitivity that remains mostly unaffected by the constraints on the sample size.

However, the use of the NV center as a high-pressure magnetic sensor suffers from some limitations, such as the implementation of the microwave excitation with the constraints associated with the DAC [5] or the detrimental influence of off-axis magnetic field that may prevent its practical use at high magnetic field [7]. These features are specific to the NV center and not to diamond in general. In particular, the silicon-vacancy (SiV) and, to a somewhat lesser

*Present address: Wainvam-e, 1 Rue Galilée, 56270 Ploemeur, France.

†Present address: Institute of Physics, Ecole Polytechnique Fédérale de Lausanne (EPFL), CH-1015 Lausanne, Switzerland.

‡Present address: Laboratoire de Physique des Matériaux et Surfaces, CY Cergy Paris Université, 95031 Cergy-Pontoise, France.

§Author to whom correspondence should be addressed: jean-francois.roch@ens-paris-saclay.fr

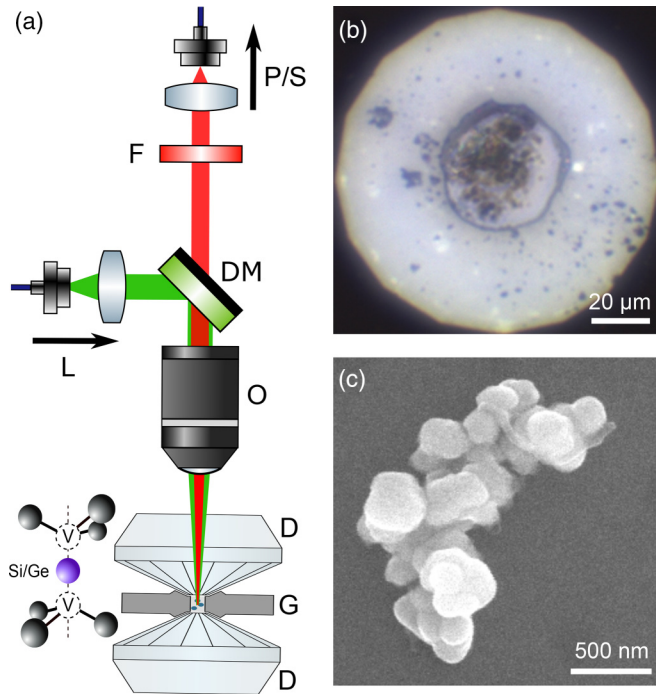


FIG. 1. (a) Description of the high-pressure experiment. SiV- and GeV-doped nanodiamonds (shown in blue) are deposited on the tip of one of the two diamonds (D) assembled in a diamond anvil cell (DAC). The geometry of the SiV and GeV centers of D_{3d} symmetry is shown on the left. The Si or Ge impurity (in purple) is linked to two vacancies (shown with dashed lines) aligned along one crystallographic axis [111] of the lattice of carbon atoms (in black). The excitation laser (L) is transmitted through an optical fiber, reflected by a dichroic mirror (DM), and then focused on the anvil tip with a microscope objective (O). The SiV/GeV photoluminescence (PL) is collected by the same objective, transmitted by the dichroic mirror, and focused in an optical fiber linked to a photon-counting detector (P) or a spectrograph (S). The remaining parasitic light from L is removed by a long-pass filter (F). (b) Image of the DAC metallic gasket (G), observed through the diamond anvil, at 8.1 GPa during the GeV spectroscopy experiment. (c) Scanning electron microscopy image of a typical cluster of GeV-doped nanodiamonds.

extent, germanium-vacancy (GeV) and tin-vacancy (SnV) centers in their negative charge state are alternative diamond point defects that have attracted considerable attention in the past decade [8]. These centers, commonly known as group-IV-vacancy (G4V) centers, share a nearly identical atomic structure. The reasons why G4V centers have potential advantages compared with the NV center are twofold. First, G4V centers exhibit extraordinary spectral stability due to their intrinsic inversion-symmetric structure as shown in Fig. 1(a) [9,10]. This property is associated with the D_{3d} point group symmetry of all G4V centers. Second, G4V centers offer the option of all-optical, microwave-free, coherent control of their spin states [11–16], allowing for applications where the use of microwave fields, as required for most NV-based sensing methods, is detrimental or technically challenging.

As a preliminary step to envisioning the use of G4V centers for high-pressure sensing, i.e., at pressures above a 100 GPa, we report here the pressure dependence of the

photoluminescence (PL) spectral properties of the SiV and GeV centers at room temperature, using doped nanodiamonds in a DAC. The evolution of the PL center wavelength with pressure for these two G4V centers is well reproduced by *ab initio* density functional theory (DFT) calculation of the PL zero-phonon line (ZPL). In these calculations the pressure dependence is computed by varying the lattice parameter according to the equation of state of diamond that can be taken as a reference for the matrix hosting the point defect [17].

II. EXPERIMENTAL SETUP

The pressure dependence of the G4V center PL spectra is investigated using nanodiamonds doped with SiV and GeV centers. The nanodiamonds were synthesized by plasma-assisted chemical vapor deposition (CVD) while introducing inside the plasma a solid silicon or germanium source in the vicinity of a molybdenum holder [18]. The number of SiV and GeV centers directly produced in the nanodiamonds can be controlled by adding N_2 and O_2 gases to the standard mixture of H_2/CH_4 used for the CVD diamond growth [19]. This method is well suited for the mass production of nanodiamonds doped with SiV or GeV centers. We estimate the incorporated color center density to a few tens of ppb, corresponding to several hundreds of color centers per nanodiamond with a typical size of about 200 nm. The nanodiamonds are then retrieved by rinsing the holder with ethanol. A drop of $\lesssim 1\mu\text{L}$ of each of these solutions is then deposited on the flattened tips of diamond anvils. The anvils, made of synthetic ultrapure diamond, are cut with Almax-Boehler design [20]. The anvil tip is a (100) crystallographic plane and has a diameter of 100 μm . After the evaporation of the ethanol solvent, clusters of the CVD-grown nanodiamonds appear on the tip, as shown in Figs. 1(b) and 1(c).

The anvils are mounted in a nonmagnetic DAC with a rhenium metallic gasket ensuring lateral confinement [Fig. 1(a)]. The DAC is loaded with neon gas as the pressure transmitting medium. The soft neon environment, which becomes solid at 4.7 GPa [21], ensures the hydrostatic compression of the nanodiamonds. The pressure in the DAC can be continuously tuned using a metallic membrane that controls the load applied on the anvils [22]. The DAC is then integrated in a customized optical confocal microscope equipped with a microscope objective (0.35 numerical aperture and 18 mm working distance) that collects the PL of the G4V centers through the diamond anvil on which the nanodiamonds have been deposited.

III. SPECTROSCOPY OF THE SILICON-VACANCY CENTER

PL spectra of seven clusters of SiV-doped nanodiamonds were recorded for increasing pressures up to 180 GPa, where the failure of an anvil induced an irreversible decompression of the DAC. The PL was excited using a single-mode cw laser at 532 nm wavelength. A ruby crystal of micrometer size was introduced in the DAC as a pressure gauge [23]. The pressure in the DAC was simultaneously determined from the shifts of the ruby PL and of the first-order Raman mode of the diamond anvil under load, following the analysis described in Ref. [24].

Figure 2 shows the spectra recorded on one cluster of SiV-doped nanodiamonds for increasing pressure steps of about

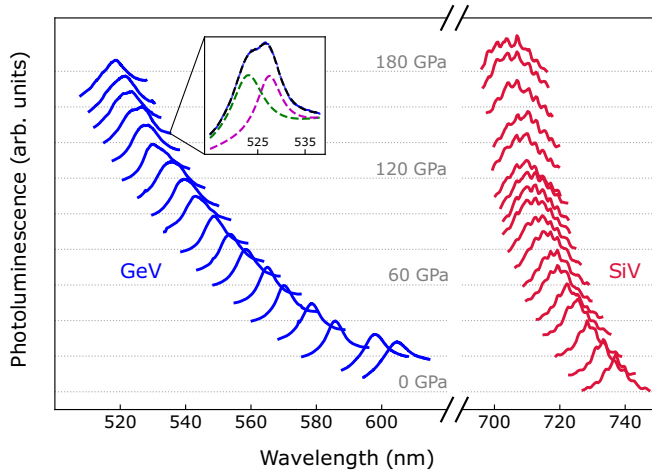


FIG. 2. Pressure dependence of the photoluminescence (PL) spectra of SiV centers (shown in red, right) and GeV centers (shown in blue, left) in CVD-grown nanodiamonds. The modulation on the SiV spectra is an artifact due to parasitic interference on the imaging detector that we first used to record the PL spectrum of the nanodiamonds. The GeV spectra were recorded with an improved spectrograph free of this artifact. The increase in pressure induces a blueshift and a broadening of the PL lines. Pressure steps for SiV are as follows (from lowest to highest curve): 1, 9, 20, 32, 40, 51, 60, 70, 79, 89, 96, 103, 110, 125, 137, 155, 171, and 180 GPa. Pressure steps for GeV are as follows (from lowest to highest curve): 8, 12, 20, 30, 40, 50, 60, 69, 79, 90, 99, 109, 119, 130, 140, 149, 157, and 168 GPa. The plots are separated vertically by the change in pressure, which is indicated by the horizontal, dotted lines. Inset: GeV spectrum recorded at 140 GPa showing its deconvolution by two shifted Lorentzian components.

10 GPa. The increase in pressure induces a blueshift of the PL line as expected from the enhanced confinement of the SiV electronic wave functions in the ground and excited states. The spectra are then fitted by a Lorentzian function in order to determine both the center emission wavelength and the linewidth. Recorded with a constant laser excitation power of 15 mW, the total PL intensity associated with a given nanodiamond slightly decreased with increasing pressure. We attribute this effect to the shift of the absorption spectrum, leading to a decrease in the absorption cross section at 532 nm wavelength.

The pressure dependence of the center energy, averaged over the seven aggregates that were investigated, is shown in Fig. 3. We estimated the error of the pressure measurement as ± 1 GPa below 79 GPa, where the pressure was accurately determined using the ruby reference, and ± 8 GPa for the Raman scattering pressure measurement that was used above 79 GPa. The statistical error of the SiV mean energy is about ± 2.5 meV for the 95% confidence interval. The graph also indicates the corresponding value of the lattice parameter inferred from the equation of state of diamond under hydrostatic conditions [17]. The results are in good agreement with previous measurements where the pressure dependence of the SiV PL was measured up to 50 GPa using nanodiamonds grown at high pressure and high temperature loaded in a DAC [25]. Although the size of the anvil tip prevented us from recording

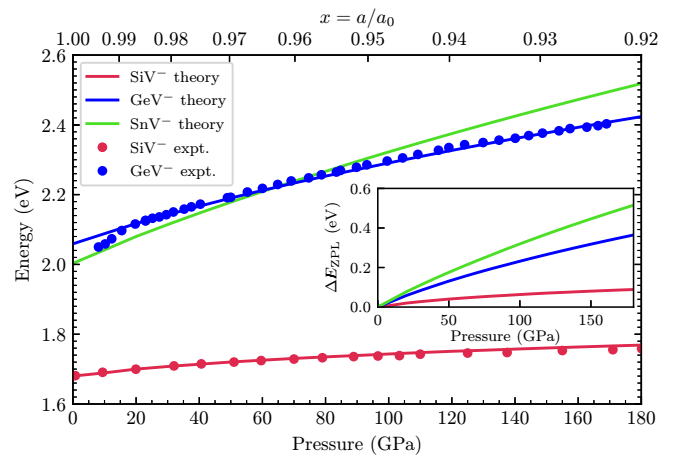


FIG. 3. Values of the PL center energies obtained from the experimental measurements of Fig. 2 for the SiV and GeV centers, plotted as a function of pressure. The error bars indicated in the main text are smaller than the size of the data points. The upper axis indicates the corresponding values of the lattice parameter ratio $x = a/a_0$, where a is the value deduced from the equation of state of diamond at a given pressure [17] and a_0 is the value at null pressure [36]. The data for the SiV and GeV centers are represented by blue and red dots, respectively. The blue and red solid curves show the results of the *ab initio* calculations of the zero-phonon line (ZPL) energy, extended to the case of the SnV center (in green). The calculated curves have been shifted to retrieve the ZPL energies at null pressure (1.68 eV for the SiV center, 2.06 eV for the GeV center, and 2.00 eV for the SnV center). The deviation observed for the GeV center below 20 GPa is attributed to a bias in the pressure estimate when we started to increase the pressure load applied to the DAC. The measurement of pressure using the Raman scattering signal is relevant only above 20 GPa, where we observe a good agreement with the result of the *ab initio* calculations. The inset shows the relative shift of the ZPL energies as calculated from the total energy differences between excited and ground states, with the influence of the growing atomic radii of the group-IV atom once embedded in the diamond lattice as an interstitial impurity.

a significant number of points at the start of the pressure exploration, the shift as a function of pressure below 20 GPa is approximately linear with a slope of about 1 meV/GPa. This value agrees with independent measurements previously performed in this weak-strain regime by bending a diamond cantilever that integrated a single SiV center [26].

Figure 2 also shows that the pressure-induced shift is associated with a broadening of the PL. Indeed the *ab initio* DFT calculation of the strain-induced ZPL shift done in Ref. [27] showed that hydrostatic pressure results in a blueshift whereas uniaxial stress results in redshifts. The broad inhomogeneous distribution of the spectral properties of SiV centers that is observed in milled or CVD-grown nanodiamonds was then explained by the uncontrolled strain environment compared with the highly reproducible properties of SiV centers designed by ion implantation in high-quality bulk diamond crystals. Such inhomogeneities could be reduced by the synthesis of high-pressure high-temperature nanodiamonds with Si or Ge precursors [28,29] or by improving the CVD growth process [30]. The PL linewidth also depends on the electron-

phonon interaction. Since the electronic states are shifted and mixed by strain, the electron-phonon scattering might be affected (see, e.g., Ref. [27]) then possibly contributing to a pressure-dependent homogeneous broadening of the PL spectrum.

IV. SPECTROSCOPY OF THE GERMANIUM-VACANCY CENTER

A similar and complementary experiment was performed by loading a DAC with GeV-doped nanodiamonds and recording the evolution of their PL with increasing pressures up to about 170 GPa. The DAC was prepared following the same procedure as previously without integrating a ruby crystal since its PL could induce a parasitic signal superimposed with the GeV PL. The pressure in the DAC was then determined from the first-order Raman mode associated with the compression of the diamond lattice, using the same analysis as in the SiV experiment [24].

Figure 2 shows the spectra recorded on a given cluster of GeV-doped nanodiamonds, exhibiting a similar behavior to that for the SiV-doped nanodiamonds. From 8 to 93 GPa, the GeV centers were excited using a single-mode cw laser at 532 nm wavelength and with a power of 75 mW. Above this pressure, the laser excitation was switched to a single-mode cw laser at 488 nm wavelength in order to compensate for the blueshift of the GeV absorption spectrum. The laser excitation power was 37 mW. The PL spectrum could then be recorded until the failure of the anvils that happened at 168 GPa. Note that above approximately 100 GPa, the PL line is split into two components as shown in the inset of Fig. 2. This splitting could be induced by the nonhydrostatic stress inside the nanodiamond which then breaks the D_{3d} symmetry that characterizes the G4V center [31,32], similarly to previous measurements realized on the NV center [33]. The experimental spectra were then fitted by two Lorentzian functions, and the PL center energy was taken as the average of the two center positions of this fit.

Figure 3 shows the evolution of the PL center energy, averaged over the three clusters of GeV-doped nanodiamonds that were investigated, as a function of the pressure in the DAC. The pressure was determined with an uncertainty of ± 1 GPa, and the statistical error of the GeV mean energy is about ± 10 meV for the 95% confidence interval. The shift with pressure is about four times faster for the GeV center than for the SiV center.

V. AB INITIO STUDY OF ZPL ENERGIES AS A FUNCTION OF PRESSURE

A. Methodology

The electronic structure and the optical excitation energies of the G4V centers in diamond can be efficiently computed using the spin-polarized DFT formalism. In the molecular-orbital picture, the ground 2E_g and excited 2E_u states of these point defects can be expressed as single Slater determinant wave functions with respective electronic configurations of $e_u^4 e_g^3$ and $e_u^3 e_g^4$ [9]. Therefore, in the framework of Kohn-Sham DFT, the energy and geometric structure of the excited 2E_u state can be calculated by employing the so-called delta-self-consistent-field (Δ SCF) approximation, whereby one e_u

electron in the lower-lying occupied Kohn-Sham level is promoted to an empty e_g level (see, e.g., Refs. [9,10,34]).

To describe the SiV and the GeV centers' electronic structure and extend it to the case of the SnV center, we used the strongly constrained and appropriately normed (SCAN) exchange-correlation functional [35], which belongs to the class of so-called meta-generalized-gradient-approximation (meta-GGA) functionals. This functional provides an accurate description of bulk diamond structural properties, yielding predictions of the diamond lattice constant $a_0 = 3.554$ Å and bulk modulus (based on the Rose-Vinet equation of state [36]) $B = 460$ GPa in close agreement with the experimental values $a_0 = 3.555$ Å [37] and $B = 446$ GPa [38]. The point defects were then modeled using $4 \times 4 \times 4$ supercells with 512 atomic sites, and the Brillouin zone was sampled at the Γ point. We used the projector-augmented wave (PAW) approach [39] as implemented in the Vienna *ab initio* simulation package (VASP) [40] with a plane-wave energy cutoff of 600 eV. Calculations for nonzero stresses are then performed by modifying the lattice constant of the defective cell according to the equation of state of diamond [17,36] using theoretical parameters calculated for bulk diamond.

B. Results

The ZPL energies at each pressure are calculated as the difference between the total energies of the excited and ground states using the Δ SCF approximation. At zero pressure, we obtain ZPL energies of 1.57, 2.00, and 1.98 eV for the negatively charged SiV, GeV, and SnV centers, respectively. These values are slightly smaller than the experimentally measured ZPL energies of 1.68, 2.06, and 2.00 eV. Note that the accuracy of the Δ SCF method with the SCAN functional is close to that of the Heyd-Scuseria-Ernzerhof (HSE) functional [10], albeit at much lower computational cost.

The calculated ZPL values of G4V centers as a pressure function are shown in Fig. 3 with solid curves. For a meaningful comparison with experiment, a constant offset is applied to the theoretical curves so that the ZPL energies at null pressure correspond to the reported experimental values. When aligned this way, the DFT results agree very well with the center energies that were previously measured for the SiV and GeV centers in all of the pressure range that was probed in the experiments.

The inset of Fig. 3 shows the relative change in theoretical ZPL energy (Δ ZPL) for the three different G4V centers as a function of pressure. We see that the rate of change is more pronounced for heavier impurity atoms with higher atomic radii. Keeping in mind the similarity of the electronic structure of all G4V defects, this naturally prompts a question regarding the reason for this difference.

C. Single-particle picture

Inspection of Kohn-Sham molecular orbital states reveals that the trend can be explained qualitatively using a single-particle picture. Indeed the single-particle energies allow for a qualitative chemical insight since the excitation energy can be roughly approximated as a difference between unoccupied and occupied states.

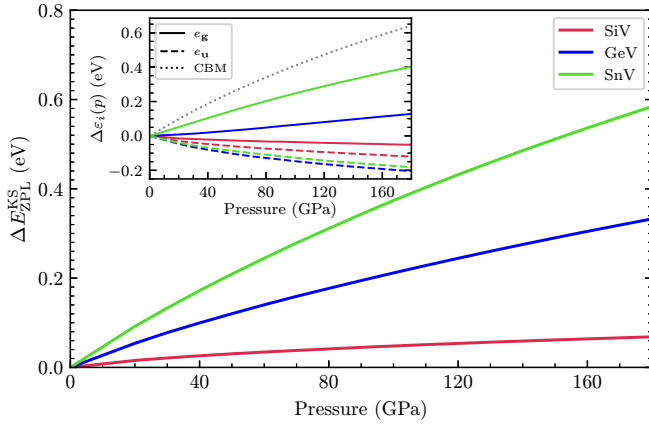


FIG. 4. Relative shift of the ZPL energies as a function of pressure as calculated from Kohn-Sham eigenvalues $\Delta E_{\text{ZPL}}^{\text{KS}}(p) = \varepsilon_{e_g}(p) - \varepsilon_{e_u}(p)$. The inset shows the relative change in the single-particle Kohn-Sham levels in the reference system of the valence band maximum (VBM). The e_g and e_u single-particle energies are represented as solid and dashed curves. The dotted gray curve denotes the conduction band minimum (CBM) as calculated in the Γ point of the $4 \times 4 \times 4$ supercell.

Figure 4 shows the relative change in the ZPL as a function of pressure as calculated from a difference between e_g and e_u single-particle energies in the electronic ground state. To investigate the orbital energy response to strain, the inset of Fig. 4 shows the change in single-particle energies in the reference system of the valence band maximum (VBM) $\Delta\varepsilon_i(p) \equiv [\varepsilon_i(p) - \varepsilon_{\text{VBM}}(p)] - [\varepsilon_i(0) - \varepsilon_{\text{VBM}}(0)]$. Here, $\varepsilon_i(p)$ is the Kohn-Sham energy of orbital ε_i at pressure p , and ε_{VBM} is the orbital energy of the VBM. One can observe that the major difference between all three G4V centers lies in the deformation potential of the e_g orbital. Based on the argument that the VBM and conduction band minimum (CBM) states are of bonding and antibonding characters [41], one can deduce that the e_g orbital changes its nature from bonding to antibonding as we increase the atomic number of the group-IV atom. An extended analysis of the difference in the electronic structure and chemical bonding of G4V centers will be given in an upcoming study.

VI. SUMMARY AND CONCLUSION

We measured the pressure dependence of the SiV and GeV PL to about 180 GPa by integrating nanodiamonds in a DAC that were doped with Si or Ge impurities during their plasma-assisted growth. The experimental results are in good agreement with *ab initio* calculations that compute the pressure dependence of the ZPL of these G4V centers according to the equation of state of diamond. This direct link suggests that SiV and GeV centers could be used as pressure calibration gauges, adding a new tool to the implementation of a practical pressure scale above a megabar [23].

The pressure dependence of the PL energies also reveals a difference between the G4V centers, being more rigidly bonded in the diamond crystal lattice for increasing atomic radii. These measurements are the first steps to determine the optical and magnetic properties of G4V centers under a broad

set of parameters that could be explored by combining high pressure and low temperature: Jahn-Teller relaxation energies, spin-orbit splitting of the ground and excited states under the influence of high stress, and the orbital relaxation rate. Lastly, charge-neutral G4V centers and, in particular, the neutral SiV⁰ center [42] could be a complementary resource since these defects can host a coherent spin that can be optically addressed with near-infrared light.

All experimental data described here are available at Zenodo [43].

ACKNOWLEDGMENTS

We are grateful to Paul Loubeyre for insightful advice and comments and to Florent Occelli for constant help and availability in handling high-pressure instrumentation. This work has received funding from the QuantERA II program under Project No. 4991922368 SENSEXTREME (Grant No. S-QUANTERA-22-1 from the Research Council of Lithuania), from the Agence Nationale de la Recherche under the project SADAHPT and the ESR/EquipEx+ program (Grant No. ANR-21-ESRE-0031), from the EMPIR program cofinanced by the participating states and the European Union's Horizon 2020 research and innovation program (20IND05 QADeT), and from the Paris Île-de-France Région in the framework of DIM SIRTEQ. Computations were performed on the super-computer GALAX of the Center for Physical Sciences and Technology, Lithuania, and on the High-Performance Computing Center "HPC Sauletekis" in the Faculty of Physics, Vilnius University. A.G. acknowledges the National Research, Development, and Innovation Office of Hungary (NKFIH; Grant No. KKP129866 of the National Excellence Program, Quantum-Coherent Materials project) and the Quantum Information National Laboratory supported by the Ministry of

TABLE I. Pressure dependence of the measured PL mean energies and computed ZPL energies for the G4V centers. The linear dependence is given in meV/GPa. Taking into account the bias in the pressure measurement at the start of the pressure load, the experimental value for the GeV center is determined between 20 and 40 GPa. Extrapolation below 20 GPa might give a result closer to the computed value due to the nonlinearity of the diamond equation of state.

	SiV center	GeV center	SnV center
	1.0	2.7	
Measured	(0–20 GPa)	(20–40 GPa)	
Computed (below 50 GPa)	1.00	2.90	3.85
Ref. [25] (below 50 GPa)	1.09		
Ref. [44] (below 6 GPa)		3.11	
Ref. [45] (below 9 GPa)			3.52
Ref. [46] (DFT)	1.1	3.2	3.5

Innovation and Technology of Hungary. The work of B.V. was funded by a Ph.D. research grant from Délégation Générale de l'Armement. J.-F.R. acknowledges support from Institut Universitaire de France.

APPENDIX

Table I compares our measured and computed values of the linear dependence of the PL mean energies and ZPL

energies in the low-pressure regime (up to 20 GPa) with previously published values. The experimental values were obtained by integrating in a DAC powders of Si-doped [25], Ge-doped [44], and Sn-doped [45] microcrystals that were synthesized from hydrocarbons at high pressures and high temperatures. The table also indicates the pressure shift that was previously computed using the QUANTUM ESPRESSO package implemented with a computational periodic supercell consisting of 83 atomic sites [46].

-
- [1] C. L. Degen, F. Reinhard, and P. Cappellaro, *Rev. Mod. Phys.* **89**, 035002 (2017).
- [2] L. Rondin, J.-P. Tetienne, T. Hingant, J.-F. Roch, P. Maletinsky, and V. Jacques, *Rep. Prog. Phys.* **77**, 056503 (2014).
- [3] M. I. Eremets, *High Pressure Experimental Methods* (Oxford University Press, Oxford, 1996).
- [4] S. Hsieh, P. Bhattacharyya, C. Zu, T. Mittiga, T. J. Smart, F. Machado, B. Kobrin, T. O. Höhn, N. Z. Rui, M. Kamrani, S. Chatterjee, S. Choi, M. Zaletel, V. V. Struzhkin, J. E. Moore, V. I. Levitas, R. Jeanloz, and N. Y. Yao, *Science* **366**, 1349 (2019).
- [5] M. Lesik, T. Plisson, L. Toraille, J. Renaud, F. Occelli, M. Schmidt, O. Salord, A. Delobbe, T. Debuisschert, L. Rondin, P. Loubeyre, and J.-F. Roch, *Science* **366**, 1359 (2019).
- [6] K. Y. Yip, K. O. Ho, K. Y. Yu, Y. Chen, W. Zhang, S. Kasahara, Y. Mizukami, T. Shibauchi, Y. Matsuda, S. K. Goh, and S. Yang, *Science* **366**, 1355 (2019).
- [7] J.-P. Tetienne, L. Rondin, P. Spinicelli, M. Chipaux, T. Debuisschert, J.-F. Roch, and V. Jacques, *New J. Phys.* **14**, 103033 (2012).
- [8] G. Thiering and A. Gali, *Diamond for Quantum Applications Part 1*, Semiconductors and Semimetals Vol. 103, edited by R. Mendelsohn and J. E. Neumann (Academic, Cambridge, MA, 2020), Chap. 1, pp. 1–36.
- [9] A. Gali and J. R. Maze, *Phys. Rev. B* **88**, 235205 (2013).
- [10] G. Thiering and A. Gali, *Phys. Rev. X* **8**, 021063 (2018).
- [11] B. Pingault, J. N. Becker, C. H. H. Schulte, C. Arend, C. Hepp, T. Godde, A. I. Tartakovskii, M. Markham, C. Becher, and M. Atatüre, *Phys. Rev. Lett.* **113**, 263601 (2014).
- [12] J. N. Becker, J. Görlitz, C. Arend, M. Markham, and C. Becher, *Nat. Commun.* **7**, 13512 (2016).
- [13] P. Siyushev, M. H. Metsch, A. Ijaz, J. M. Binder, M. K. Bhaskar, D. D. Sukachev, A. Sipahigil, R. E. Evans, C. T. Nguyen, M. D. Lukin, P. R. Hemmer, Y. N. Palyanov, I. N. Kupriyanov, Y. M. Borzdov, L. J. Rogers, and F. Jelezko, *Phys. Rev. B* **96**, 081201(R) (2017).
- [14] J. N. Becker, B. Pingault, D. Groß, M. Gündoğan, N. Kukharchyk, M. Markham, A. Edmonds, M. Atatüre, P. Bushev, and C. Becher, *Phys. Rev. Lett.* **120**, 053603 (2018).
- [15] C. Weinzelt, J. Görlitz, J. N. Becker, I. A. Walmsley, E. Poem, J. Nunn, and C. Becher, *Phys. Rev. Lett.* **122**, 063601 (2019).
- [16] R. Debroux, C. P. Michaels, C. M. Purser, N. Wan, M. E. Trusheim, J. A. Martínez, R. A. Parker, A. M. Stramma, K. C. Chen, L. de Santis, E. M. Alexeev, A. C. Ferrari, D. Englund, D. A. Gangloff, and M. Atatüre, *Phys. Rev. X* **11**, 041041 (2021).
- [17] F. Occelli, P. Loubeyre, and R. Letoullec, *Nat. Mater.* **2**, 151 (2003).
- [18] M. D. Feudis, A. Tallaire, L. Nicolas, O. Brinza, P. Goldner, G. Hétet, F. Bénédic, and J. Achard, *Adv. Mater. Interfaces* **7**, 1901408 (2020).
- [19] A. Tallaire, O. Brinza, M. De Feudis, A. Ferrier, N. Touati, L. Binet, L. Nicolas, T. Delord, G. Hétet, T. Herzig, S. Pezzagna, P. Goldner, and J. Achard, *ACS Appl. Nano Mater.* **2**, 5952 (2019).
- [20] R. Boehler and K. D. Hantsetters, *High Pressure Res.* **24**, 391 (2004).
- [21] W. L. Vos, J. A. Schouten, D. A. Young, and M. Ross, *J. Chem. Phys.* **94**, 3835 (1991).
- [22] R. Letoullec, J. P. Pinceaux, and P. Loubeyre, *High Pressure Res.* **1**, 77 (1988).
- [23] G. Shen, Y. Wang, A. Dewaele, C. Wu, D. E. Fratanduono, J. Eggert, S. Klotz, K. F. Dziubek, P. Loubeyre, O. V. Fat'yanov, P. D. Asimow, T. Mashimo, R. M. M. Wentzcovitch *et al.* (IPPS Task Group), *High Pressure Res.* **40**, 299 (2020).
- [24] Y. Akahama and H. Kawamura, *J. Appl. Phys.* **96**, 3748 (2004).
- [25] S. Lyapin, I. Ilichev, A. Novikov, V. Davydov, and V. Agafonov, *Nanosyst.: Phys. Chem. Math.* **9**, 55 (2018).
- [26] S. Meesala, Y.-I. Sohn, B. Pingault, L. Shao, H. A. Atikian, J. Holzgrafe, M. Gündoğan, C. Stavrakas, A. Sipahigil, C. Chia, R. Evans, M. J. Burek, M. Zhang, L. Wu, J. L. Pacheco, J. Abraham, E. Bielejec, M. D. Lukin, M. Atatüre, and M. Lončar, *Phys. Rev. B* **97**, 205444 (2018).
- [27] S. Lindner, A. Bommer, A. Muzha, A. Krueger, L. Gines, S. Mandal, O. Williams, E. Londero, A. Gali, and C. Becher, *New J. Phys.* **20**, 115002 (2018).
- [28] V. A. Davydov, A. V. Rakhmanina, S. G. Lyapin, I. D. Ilichev, K. N. Boldyrev, A. A. Shiryayev, and V. N. Agafonov, *JETP Lett.* **99**, 585 (2014).
- [29] C. T. Nguyen, R. E. Evans, A. Sipahigil, M. K. Bhaskar, D. D. Sukachev, V. N. Agafonov, V. A. Davydov, L. F. Kulikova, F. Jelezko, and M. D. Lukin, *Appl. Phys. Lett.* **112**, 203102 (2018).
- [30] F. Isa, M. Joliffe, B. Wouterlood, N. H. Ho, T. Volz, A. Bendavid, and L. J. Rogers, *arXiv:2208.08075*.
- [31] A. E. Hughes and W. A. Runciman, *Proc. Phys. Soc.* **90**, 827 (1967).
- [32] C. Hepp, T. Müller, V. Waselowski, J. N. Becker, B. Pingault, H. Sternschulte, D. Steinmüller-Nethl, A. Gali, J. R. Maze, M. Atatüre, and C. Becher, *Phys. Rev. Lett.* **112**, 036405 (2014).
- [33] F. Grazioso, B. R. Patton, P. Delaney, M. L. Markham, D. J. Twitchen, and J. M. Smith, *Appl. Phys. Lett.* **103**, 101905 (2013).

- [34] E. Londero, G. Thiering, L. Razinkovas, A. Gali, and A. Alkauskas, *Phys. Rev. B* **98**, 035306 (2018).
- [35] J. Sun, A. Ruzsinszky, and J. P. Perdew, *Phys. Rev. Lett.* **115**, 036402 (2015).
- [36] P. Vinet, J. R. Smith, J. Ferrante, and J. H. Rose, *Phys. Rev. B* **35**, 1945 (1987).
- [37] P. Hao, Y. Fang, J. Sun, G. I. Csonka, P. H. T. Philipsen, and J. P. Perdew, *Phys. Rev. B* **85**, 014111 (2012).
- [38] E. S. Zouboulis, M. Grimsditch, A. K. Ramdas, and S. Rodriguez, *Phys. Rev. B* **57**, 2889 (1998).
- [39] P. E. Blöchl, *Phys. Rev. B* **50**, 17953 (1994).
- [40] G. Kresse and J. Furthmüller, *Phys. Rev. B* **54**, 11169 (1996).
- [41] W. A. Harrison, *Electronic Structure and the Properties of Solids: The Physics of the Chemical Bond* (Courier, Chelmsford, MA, 2012).
- [42] B. C. Rose, D. Huang, Z.-H. Zhang, P. Stevenson, A. M. Tyryshkin, S. Sangtawesin, S. Srinivasan, L. Loudin, M. L. Markham, A. M. Edmonds, D. J. Twitchen, S. A. Lyon, and N. P. de Leon, *Science* **361**, 60 (2018).
- [43] B. Vindolet, M.-P. Adam, L. Toraille, M. Chipaux, A. Hilberer, L. Razinkovas, A. Alkauskas, G. Thiering, A. Gali, M. De Feudis, M. W. Ngandeu Ngambou, J. Achard, A. Tallaire, M. Schmidt, C. Becher, and J.-F. Roch, Zenodo (2022), <https://doi.org/10.5281/zenodo.7086416>.
- [44] S. G. Lyapin, A. A. Razgulov, A. P. Novikov, E. A. Ekimov, and M. V. Kondrin, *Nanosyst.: Phys. Chem. Math.* **9**, 67 (2018).
- [45] A. Razgulov, S. Lyapin, A. Novikov, and E. Ekimov, *Diamond Relat. Mater.* **116**, 108379 (2021).
- [46] E. A. Ekimov, S. G. Lyapin, A. A. Razgulov, and M. V. Kondrin, *J. Exp. Theor. Phys.* **129**, 855 (2019).